Cyclic Deformation, Dislocation Structure, and Internal Fatigue Crack Generation in a Ti-Fe-O Alloy at Liquid Nitrogen Temperature

H. YOKOYAMA, O. UMEZAWA,* K. NAGAI, T. SUZUKI, and K. KOKUBO

To clarify the internal fatigue crack generation in a Ti-Fe-O (near α-type) alloy, microstructures, internal fatigue crack initiation sites, and dislocation structures in samples fractured during high-cycle fatigue tests at liquid nitrogen temperature were studied. The alloy contained two kinds of elongated α-phase microstructures, *i.e.*, recovered α grains and recrystallized α grains. Untested samples contained mobile dislocations in recovered α grains, but in recrystallized α grains, any dislocations were observed. Internal crack initiation sites were formed transgranularly and were related to the recrystallized α grain region, judging from their morphology, size, and chemistry. Dislocations in recovered α grains were rearranged after cyclic loading in either $\{01\bar{1}0\} - \langle 11\bar{2}0\rangle$ planar arrays or subgrain structures due to dislocation annihilation. Few dislocations were seen in recrystallized α grains. We discuss the relationship between localized strain incompatibility due to coplanar arrays in recovered α grains and transgranular cracking in recrystallized α grains, and propose a model for fatigue crack generation.

I. INTRODUCTION

FATIGUE crack initiation is generally understood to occur on a specimen surface due to irreversible process of extrusion and intrusion through slip deformation.[1] Some high strength alloys such as titanium alloys and nitrogen-strengthened austenitic steels, however, clearly exhibit two kinds of fatigue crack initiation at and below room temperature, *e.g.*, 4, 77, and 300 K.[2] One is at the specimen surface, and the other is in the specimen interior. The internal (subsurface) crack initiation is not associated with pre-existing defects such as nonmetallic inclusions and foreign elements. This fracture mechanism cannot be explained by extrusion-intrusion (persistent slip bands) models.[3,4] Internal fatigue crack initiation is dominant in the high cycle fatigue regime and at lower temperatures, while surface cracks are initiated in high peak stress and low cycle fatigue tests. The initiation site thus shifts from the surface to the interior at lower stress, and the internal crack initiation behavior can be clearly detected at cryogenic temperatures. Generally, the tensile strength of alloys is increased as the temperature is decreased. It appears that low-temperature (cryogenic) fatigue tests make clear the features of fatigue crack generation behavior in high-strength alloys such as Ti-6Al-4V,[5] Ti-5Al-2.5Sn,[6] and austenitic steels.[7]

The place most likely for the internal crack initiation sites is near the specimen surface where macroscopic deformation is localized.[8,9] For example, internal sites of Ti-6Al-4V alloys were mostly placed a few hundred microns deep from the specimen surface.[10,11,12] Such heterogeneity of macroscopic deformation in a sample may affect the location of internal crack initiation sites. Some exceptions such as much deeper locations, however, have been reported in alloys such as β-quenched Ti-6Al-4V[12] and austenitic steels.[11] In both cases, the size of crack initiation site (facet) was over a few tens of microns in diameter and much larger than that in Ti-6Al-4V alloys.

The Ti-Fe-O-(N) based alloy, which is a near α-type titanium alloy, has been proposed for a new high-strength titanium alloy.[13] The alloy derives its strength from solid-solution hardening by interstitial elements such as oxygen and nitrogen. The supersaturation of iron leads to retention of β phase, which is effective to refine α matrix structure. In the previous article,[12] the Ti-Fe-O alloy showed the internal crack initiation at 77 K and no depth favoring of the location. No defects such as inclusions or pores were seen in the internal crack initiation sites, and their fractographic features were similar to those in Ti-6Al-4V alloys. The internal crack initiation in the Ti-Fe-O alloy, however, was insensitive to the heterogeneity of macroscopic deformation.

Terms such as quasi-cleavage, cleavage, and slip plane decohesion have been used to describe microscale fractographic features of the internal initiation sites in Ti-6Al-4V alloys.[5,14,15] Planar dislocations piled up in the vicinity of grain boundaries have been shown to cause transgranular cracking in α grains.[6,15] Slip planarity is favored not only by low stacking fault energy, but also by shear modulus, atomic size misfit, solute content, short-range order, and dispersion particles.[16,17] Thus, internal crack initiation must be related to the size of the initiation site,[18] applied stress,[10] and microstructural factors[5,11,18,19] such as grain size, distribution, chemistry, and texture. In studies of internal crack initiation for a Ti-5Al-2.5Sn extra-low interstitials (ELI) alloy,[20] localized slip in a specific inhomogeneous microstructure was related to a potential source of the microcrack

H. YOKOYAMA, formerly Graduate Student, Department of Mechanical Engineering, Kogakuin University, is Engineer, Nittan Valve Co. Ltd., Kanagawa 257-0031, Japan. O. UMEZAWA, Senior Scientist, and K. NAGAI, Unit Leader, are with the Frontier Research Center for Structural Materials, National Research Institute for Metals, Ibaraki 305-0047, Japan. T. SUZUKI, Emeritus Professor, and K. KOKUBO, Professor, are with the Department of Mechanical Engineering, Kogakuin University, Tokyo 163-8677, Japan.

*To whom all correspondence should be addressed.

Manuscript submitted November 9, 1999.

Table I. Chemical Compositions of Ti-Fe-O Alloy in Mass Percent

C	Fe	N	O	H	Ti
0.015	0.71	0.0158	0.269	0.001	bal

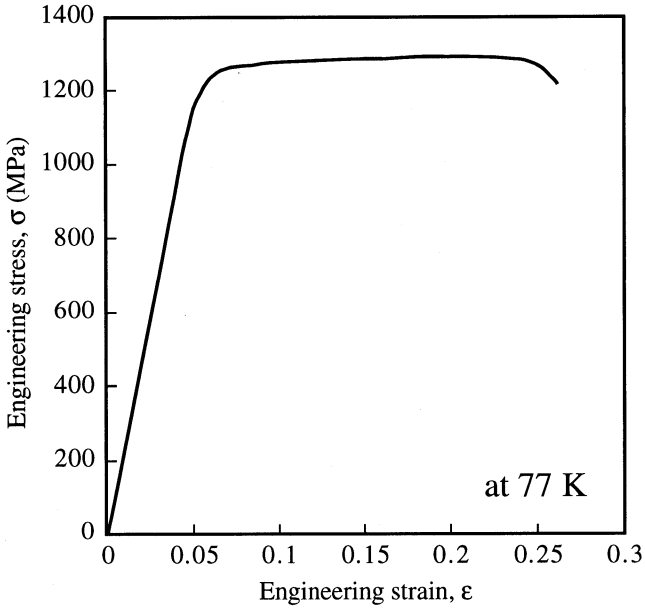

Fig. 1—Engineering stress *vs* engineering strain curve at 77 K for the Ti-Fe-O alloy.

generation. To clarify the mechanism of internal crack generation, therefore, it is important to understand local strain incompatibility related to microstructural heterogeneity.

The objective of the present article is to identify the features of internal crack initiation in the Ti-Fe-O alloy at 77 K and to discuss models for the internal fatigue crack generation. Hence, the microstructure and internal fatigue crack initiation sites of the Ti-Fe-O alloy are characterized, and the deformation structure in investigated for the fatigue.

II. EXPERIMENTAL

A. *Test Materials*

The test material was a mill-annealed plate of a near α-type Ti-Fe-O alloy; the chemical compositions are given in Table I. The Ti-Fe-O alloy was melted in a laboratory scale, hot-forged in β region (1223 K heating), and hot-rolled in α region (1073 K heating) to a 30-mm-thick plate.

Figure 1 shows an engineering stress *vs* engineering strain curve for the alloy at 77 K. Tensile tests were done at a strain rate of 8.33×10^{-4} s^{-1} using a screw-driven-type tester. Cylindrical test pieces were cut parallel to the rolling direction (RD); the gage geometry was 3.5 mm in diameter and 20 mm in length. Tensile properties at 77 K are submitted by duplicate tests as follows; 0.2 pct proof stress: 1165 MPa, ultimate tensile strength: 1292 MPa, and elongation: 21.6 pct.

Fatigue test specimens were machined parallel to the RD,

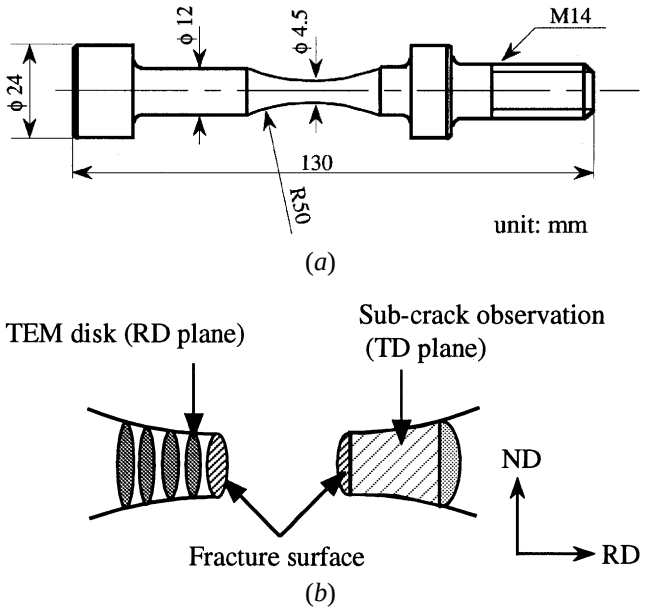

Fig. 2—Configurations of (*a*) fatigue test specimen and (*b*) test samples. The ND, RD, and TD are indicated in (b).

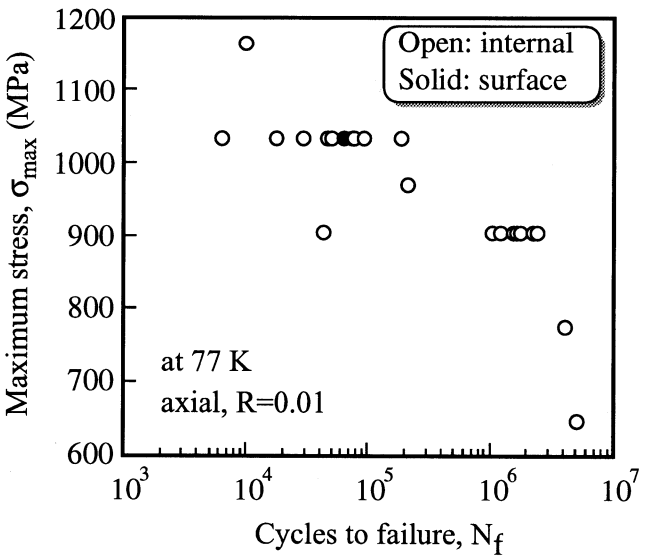

Fig. 3—S–N data of the Ti-Fe-O alloy at 77 K.[12]

and their configuration is shown in Figure 2(a). Fatigue testing was carried out with the specimen immersed in liquid nitrogen (77 K).[12] Using a cryogenic servohydraulic fatigue machine,[21] load-controlling tests were done. The sinusoidal waveform loading was uniaxial with a minimum-to-maximum stress ratio, R ($\sigma_{min}/\sigma_{max}$), of 0.01. Test frequency of 10 Hz was chosen so that the specimen temperature rise should be as low as possible.[22] Figure 3 shows S–N (maximum stress *vs* number of cycles) data.[12] Most samples exhibited internal crack initiation (open plots in Figure 3). Their maximum cyclic stress was much lower than macroyield stress (Figure 1).

B. *Analysis*

Fatigue crack initiation sites and fracture surfaces were studied by scanning electron microscopy (SEM) and energy

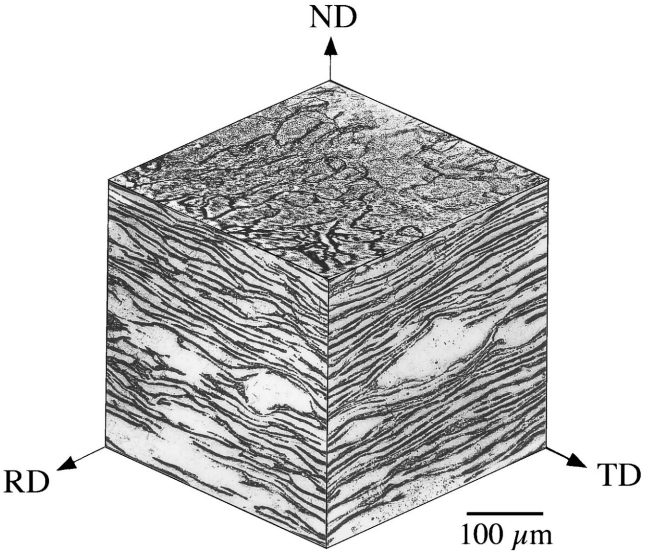

(*a*)

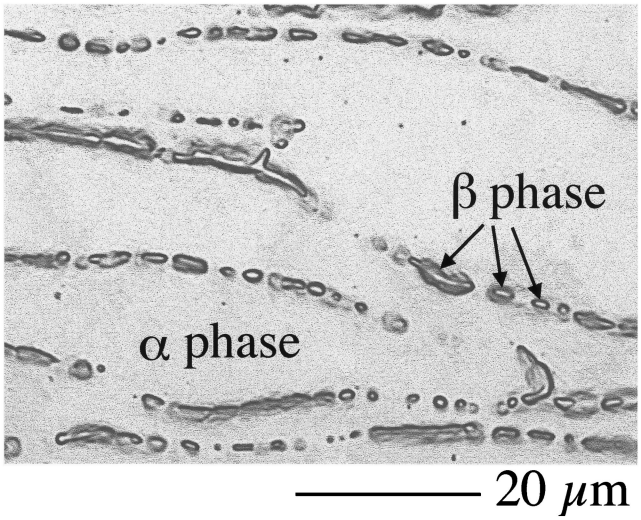

(*b*)

Fig. 4—(*a*) Optical micrographs of the Ti-Fe-O alloy and (*b*) a magnified photograph on the RD plane.

dispersive X-ray spectroscopy (EDS). The microscope is a JEOL* JSM-6400 equipped with a LaB_6 type gun. Subcracks were analyzed in the longitudinal cross section on the transverse direction (TD) plane (Figure 2(b)). Electron backscatter diffraction pattern (EBSP) analysis in SEM[23] was used to determine the α-phase microstructure. Data sets of point analysis with every 0. 2 μm beam scanning for both *X* and *Y* (parallel to the principal stress axis) directions yielded several kinds of image analyses, *e.g.*, image quality and orientation by a tiled inverse pole figure. Low confidence data with less than 0.4 in confidence index (CI), which ranges between 0 (none) and 1 (perfect),[23] were omitted for the orientation analysis. The microstructure and dislocation structure were studied by transmission electron microscopy (TEM). The TEM disks were sectioned from beneath the fracture surface (Figure 2(b)) perpendicular to the principal stress axis and mechanically ground. Each disk diameter was measured and its maximum cyclic stress, σ_{max}, was calibrated, since the fatigue test specimens had an hourglass shape. The TEM foils were prepared by electrochemical twin-jet polishing at 243 K in a stirred solution of 6 pct perchloric acid, 35 pct butanol, and 59 pct methanol. A JEOL 2000FXII electron microscope equipped with a double tilt goniometer stage was used at 200 keV. The nature of the dislocation was determined using the standard $g \cdot b$ analysis technique, under two beam condition.

*JEOL is a trademark of Japan Electron Optics Ltd., Tokyo.

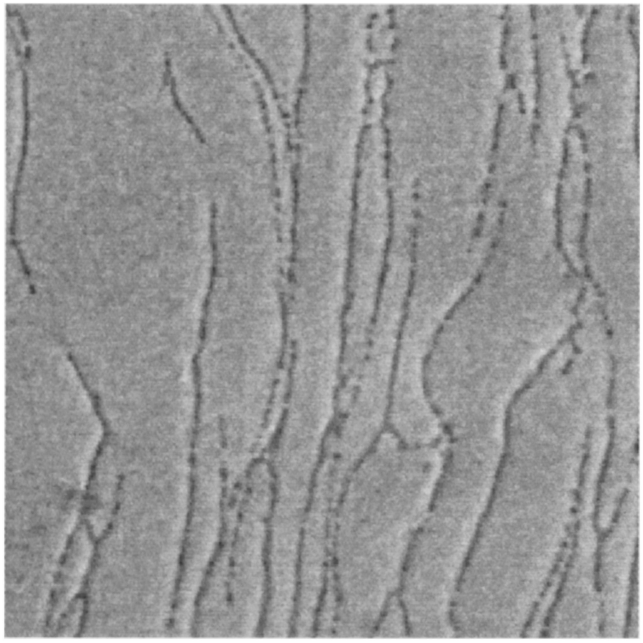

(*a*)

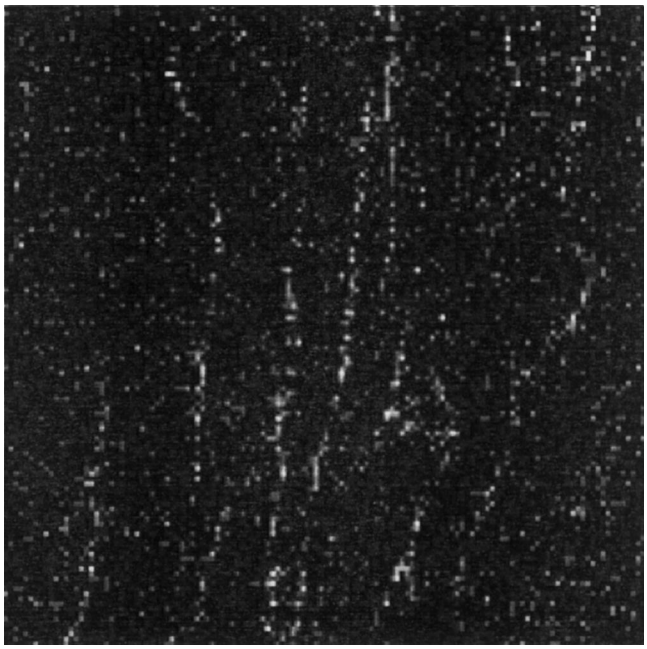

(*b*)

Fig. 5—(*a*) Secondary electron image on the RD plane and (*b*) its iron mapping image by EDS.

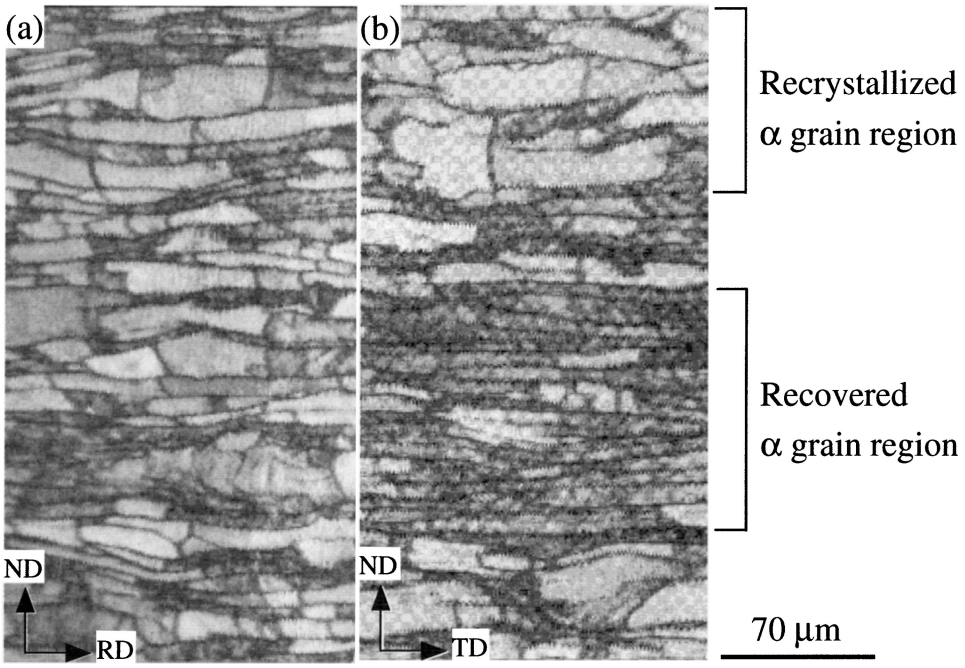

Fig. 6—EBSP image quality maps for (*a*) TD and (*b*) RD planes.

III. RESULTS

A. *As-Received Microstructure*

A combination of optical micrographs with normal direction (ND), RD, and TD is shown in Figure 4(a). The alloy consisted of α and fine retained β phases. Beta particles are distributed along α grain boundaries (Figure 4(b)). Iron is a strong β former element in titanium alloys and is concentrated at some α grain boundaries (Figure 5). No iron was detected in α phase and oxygen was enriched in α phase. Thus, iron was enriched in the β particles distributed along α grain boundaries. Alpha grains are elongated in both RD and TD (Figure 4(a)). In the image quality map shown in Figure 6, the microstructure is classified into two regions, which are designated as recrystallized α grain and recovered α grain. Since the image quality of EBSP reflects the perfection of a crystal, strain and defects such as dislocations cause poor quality (*i.e.*, dark in the image quality maps). A recrystallized α grain region thus shows higher quality than a recovered α grain one. In fact, the recovered α grain region is darker gray than the recrystallized α one in Figure 6. The α grain width in the recovered α grain region is about several microns, compared to about 20 μm in the recrystallized α one. Figure 7 shows the contour inverse pole figure of the TD plane shown in Figure 6(a), corresponding to the orientation from (a) TD, (b) RD, and (c) ND. Each α grain elongates parallel to the RD, but does not have a strong texture. Recrystallized α grains have a large angle boundary between neighboring α grains. Recovered α grains showed dislocation loops and dislocations in subgrains, as shown in Figure 8, although few dislocations were observed in recrystallized α grains. The dislocations are not tangled, and no slip bands were observed. As a result of hot rolling and mill-annealed condition, partially recrystallized α phase structure may be obtained.

B. *Fatigue Crack Initiation Site*

No defects such as inclusions or pores were detected at internal crack initiation sites (Figure 9). The fracture surface is classified into three sections, *i.e.*, regions I, II, and III, as illustrated in Figure 9(b). A fatigue crack is initiated internally and forms a crystallographic facet (region I) that propagates in a radial pattern in region II (Figure 9(c)). Subcracks with crystallographic facets are seen in region II (Figure 9(d)), and separations are detected in region III. The crack initiation site (region I), subcracks, and separations are aligned along the TD. The internal crack initiation site is flat at low magnification and inclined to the principal stress axis (Figure 9(c)).

Initiation sites consisted of one or more facets. Figure 10 shows the matching halves of an internal crack initiation site formed at a higher maximum stress. The internal crack initiation site is a crystallographic facet. Region A marked in Figures 10(c) and (d) has no traces and/or protrusions and contacts the edge of the initiation site. The rest of region A in the site, region B, involves traces or steps on the facet. Traces grew radially from region A. The inclination of regions A and B in Figure 10 with respect to the principal stress axis was almost the same.[24] Figure 11 shows the iron mapping by EDS. The iron-enriched region, *i.e.*, lines CC′ and DD′, is fitted to the edge of the initiation site. Iron was enriched in the β particles distributed along α grain boundaries. Judging from the shape, size, and iron distribution, the initiation site is fitted to a recrystallized α grain region.

Figure 12 shows an internal crack initiation site of a sample that failed at the lowest applied stress level in the present study. Several facets form the initiation site, which is larger than that at higher stress. Each facet in Figure 12 is inclined roughly the same.[24]

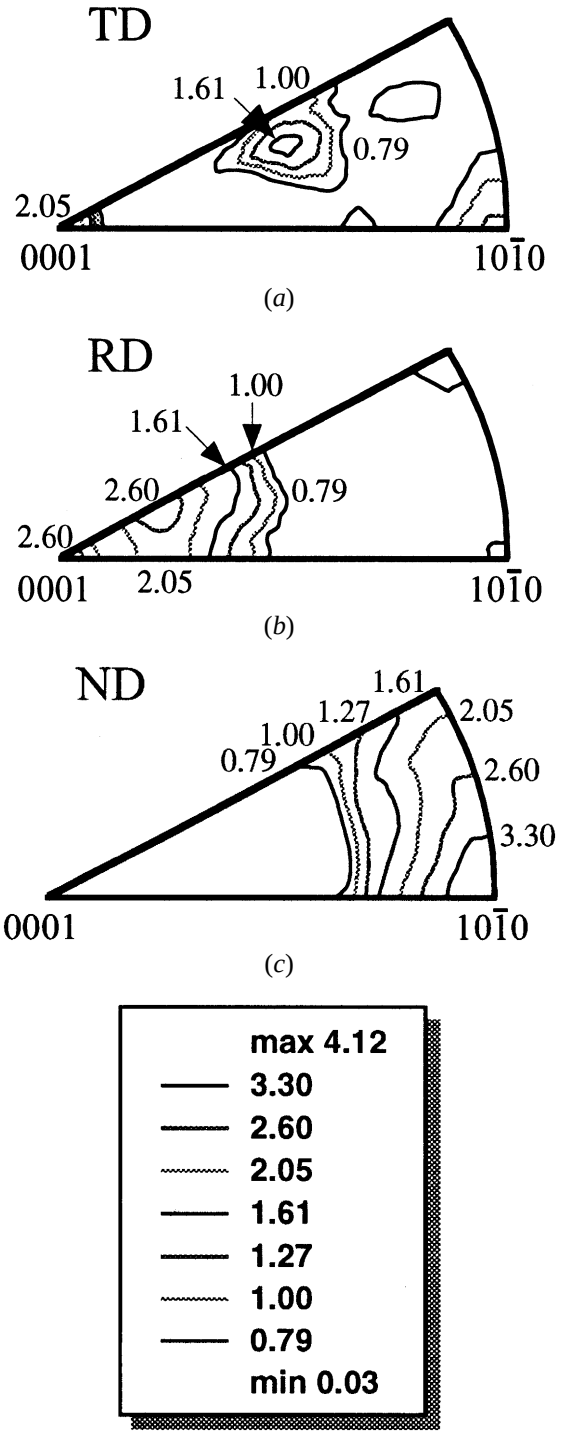

Fig. 7—Contour inverse pole figure for EBSP readings taken from Fig. 6(a): (*a*) TD, (*b*) RD, and (*c*) ND.

C. *Subcracks*

Figure 13 shows subcracks on the TD plane (in the longitudinal section) for a fractured sample. Comparing images with secondary electron (a), image quality (b), and orientation mapping (c), grain boundaries, deformation (slip) bands, α grain structures, and cracks are clearly recognized in the microstructure. Subcracks, a few tens of microns long, are detected in a recrystallized α grain region and are inclined to the principal stress axis by about 30 deg. The subcracks form transgranularly, and a subcrack goes through a grain boundary over two grains in a recrystallized α grain region. Thus subcracks are generated almost parallel to each other (Figure 13(b)). The EBSP readings were taken from the regions marked as 1, 2, 3, and 4 in Figure 13(b) near the subcracks. They are illustrated in the corresponding discrete inverse pole figure of Figure 13(c). The pole figure demonstrates that the polished vertical sections (TD plane) of grains in which the subcracks have developed are oriented at about 80 deg away from the basal plane. It can be deduced that the facet plane of the subcracks has a near basal orientation, since the subcracks were developed along the TD, as shown in Figure 9(b).

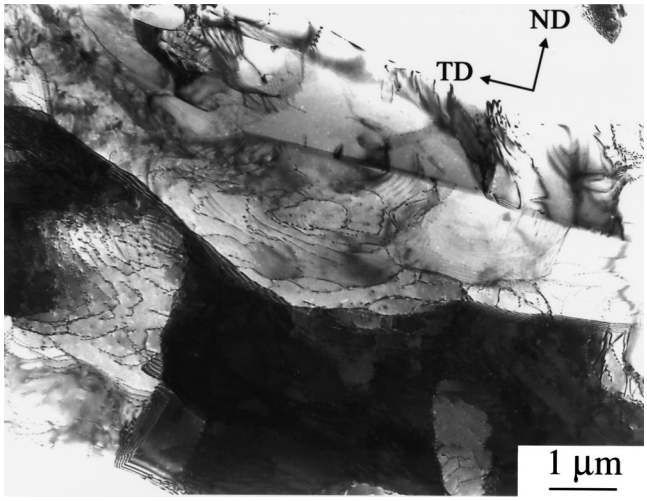

Fig. 8—Dislocations in recovered α grains of the Ti-Fe-O alloy. The beam direction is near (01$\bar{1}$0).

Traces of slip bands occur in recovered α grains, and only a few of them are detected near grain boundaries in recrystallized α grains. Those are also inclined to the principal stress axis at about 30 to 60 deg.

D. *Dislocation Structures*

The TEM micrographs (Figures 14(a) and (b)) as well as optical micrographs in Figure 4(b) show that β phases are ellipsoidal and several hundreds of nanometers wide. Most of the β particles are aligned discontinuously along α grain boundaries.

Coplanar arrays occur preferentially only in recovered α grains (Figures 14(a) and (b)). The dominant deformation mode is *via* the $\{01\bar{1}0\} - \langle 11\bar{2}0\rangle$ slip system, and the glide process is markedly planar. Nearly all the dislocations observed are screw type, and the movement is restricted on their slip planes. Thus, cross-slip from a prism plane onto another is difficult. The slip can go through subgrain boundaries in the recovered α grains, as shown in Figure 14(a). However, the arrays are blocked at grain boundaries neighboring recrystallized α grain (Figure 14(b)). When a dislocation source emits a series of dislocations all lying on the same slip plane, dislocations pile up behind the leading dislocation and interact elastically. Sets of dislocations are observed where four or five dislocations are stacked (Figure 14(c)). The sets of stacked dislocations lie between 90 and

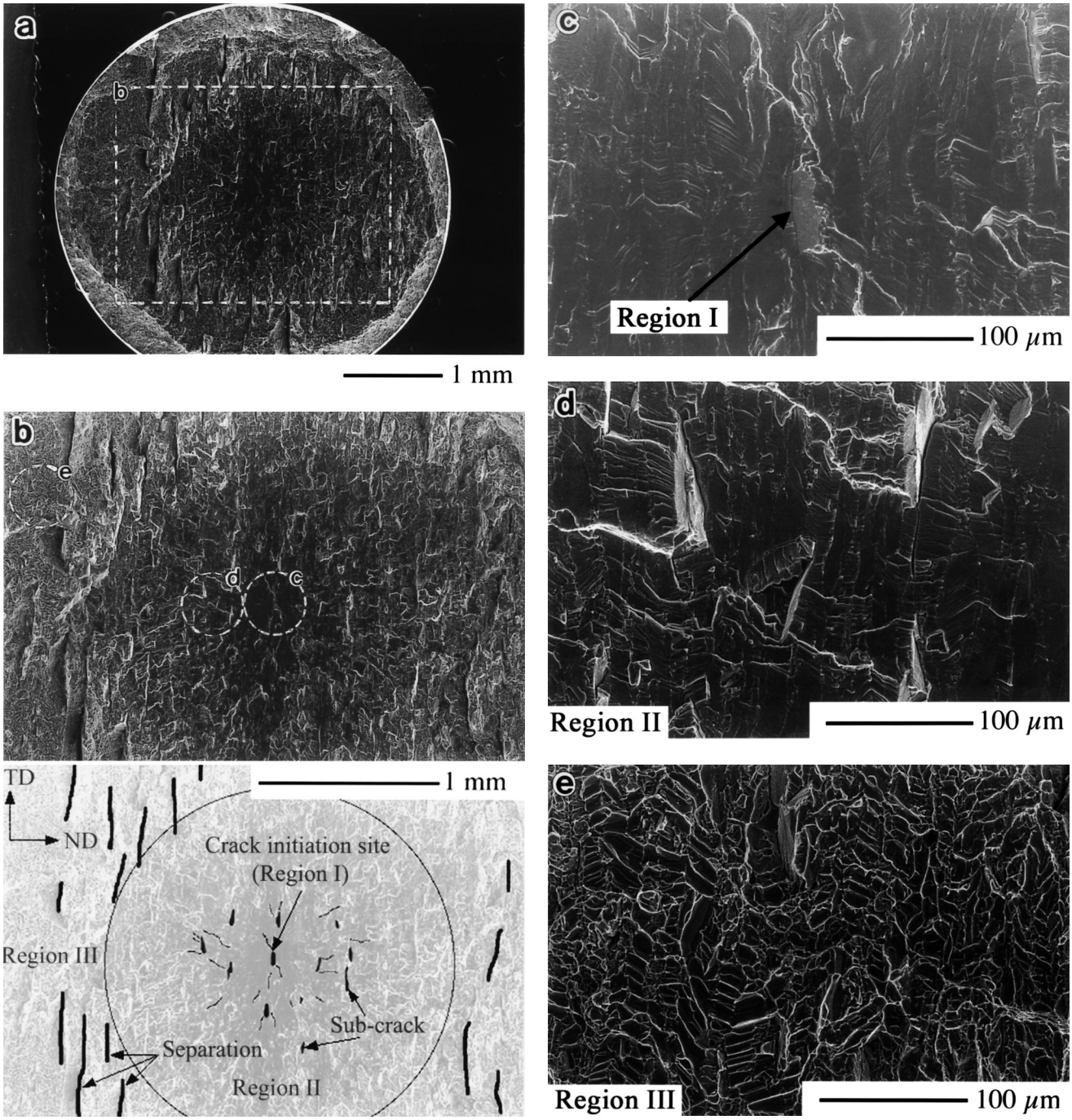

Fig. 9—SEM photographs of fracture surface in a sample showing internal crack initiation (σ_{max} = 1033 MPa, N_f = 74,650 cycles): (*a*) whole image of fracture surface, (*b*) fatigue fracture surface and its illustration showing three sections, (*c*) magnified image near the crack initiation site (region I), (*d*) magnified image in region II, and (*e*) magnified image in region III.

130 nm on the *x*-axis at even intervals. The stacked dislocations are due to active parallel slip planes, because preexisting dislocations can give sources of arrays on parallel slip planes. Suppose two parallel screw dislocations, one along the *z*-axis, as illustrated in Figure 14(c). The *x* component of force on the other is

$$f(x) = \frac{\mu b_1 b_2}{2\pi} \frac{x}{x^2 + y^2} \qquad [1]$$

where μ is the shear modulus. The $f(x)$ is repulsive for screws of the same sign, and its maximum is given under the condition $x = y$ or $x = -y$,

$$f(x)_{max} = \frac{\mu b_1 b_2}{4\pi x} \; (x > 0) \qquad [2]$$

If slip planes are parallel to the *x*-axis, the *x* component of the distance between neighboring dislocations in a set of stacked dislocations is about 30 nm. Based on Eq. [2], the distance is reasonable, because it is almost comparable to foil thickness. In Eq. [2], the *x* component of maximum

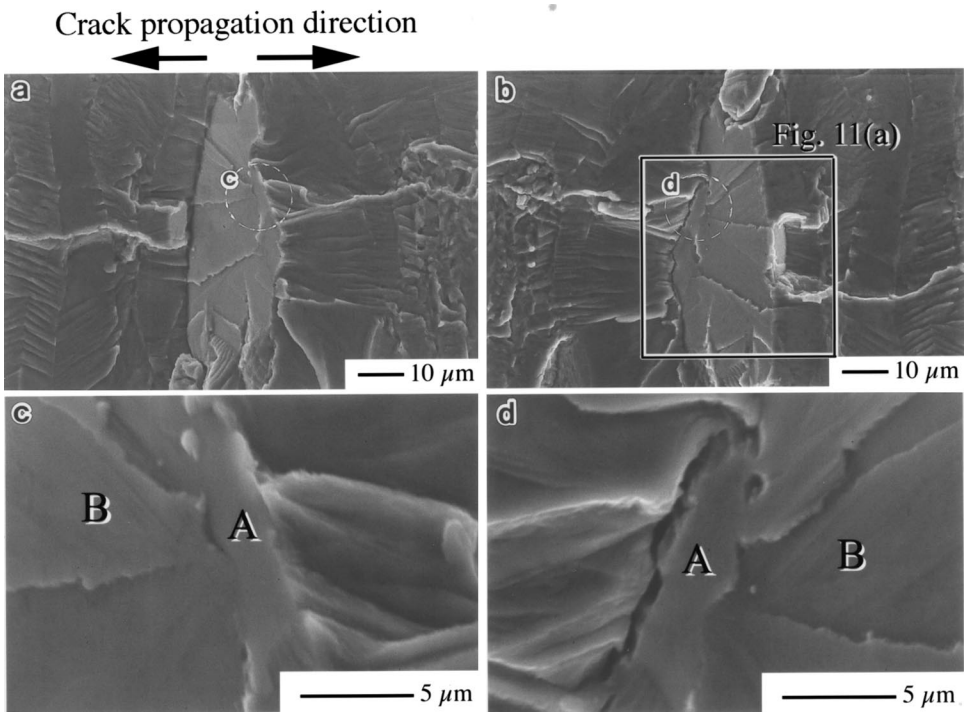

Fig. 10—Matching halves near an internal crack initiation site (σ_{max} = 1033 MPa, N_f = 186,590 cycles); photographs (*c*) and (*d*) are magnified images of photographs (*a*) and (*b*).

force is estimated to be about 9×10^{-3} (N/m), where $\mu = 39.8 \times 10^9$ (N/m^2), $b = 2.94 \times 10^{-10}$ (m), and $x = 30 \times 10^{-9}$ (m) are adopted.

During the fatigue process, subgrain structures further develop in recovered α grains, as shown in Figure 15. The subgrain boundaries are aligned about 400 nm apart. Dislocations remain within subgrains, although annihilation and rearrangement of pre-existing dislocations are responsible for developing sub-boundaries.

Almost no dislocations are observed in recrystallized α grains (Figure 16) even after fatigue fracture, although dislocations covered both recovered and recrystallized α grains in the tensile fractured specimen at 77 K.

Traces of slip bands (Figure 13(b)) and coplanar dislocation arrays were well developed in the recovered α grains, indicating that glide processes are active mostly in recovered α grains and that pre-existing dislocations are mobile.

IV. DISCUSSION

Internal fatigue crack initiation models based on dislocation pileups in the α phase have been proposed for Ti-6Al-4V alloys. Neal and Blenkinsop[15] noted that piled-up dislocations on $\{10\bar{1}0\}_\alpha$ cause cleavage on the $\{10\bar{1}7\}_\alpha$ plane by the Stroh mechanism,[25] but the model did not appear to be geometrically correct.[14] An alternative mechanism postulated by Ruppen *et al.*[14] assumes a $(001)_\beta$ cleavage crack caused by pileups on $\{10\bar{1}0\}_\alpha$, but no experimental evidence was found for a cleavage crack in the β phase. On the other hand, multiple slips were detected in the β phase rather than in the α phase.[2] Brittle microcracking in the β phase may thus not be responsible for internal fatigue crack initiation. Umezawa *et al.*[5] suggest that a facet is created not by instantaneous spread of crack but by microcrack growth in the α phase involving a large number of cycles. Sarrazin *et al.*[26] showed that internal crack initiation site was characterized by a fracture on the basal plane of α phase. In the present study, EBSP analysis has reinforced the view that the facets of subcracks shown in Figure 13 have a near basal plane orientation with respect to the hexagonal crystal lattice. This result is consistent with the previous works,[26–30] in near α titanium alloys. It has been suggested that short fatigue cracks propagate along a path where the basal planes of adjacent α grains are parallel to each other.[27] For near α titanium alloys at low temperature, however, the basal plane in α phase can hardly be associated with dislocation movement.[31,32] Nevertheless, Wojcik *et al.*[33] suggested that facet formation requires a critical combination of shear stress (*i.e.*, basal slip) and tensile stress normal to the slip plane.

The microstructure of the Ti-Fe-O alloy was classified into two regions: recrystallized and recovered α grains. In the present study, the initiation site can be identified as transgranular cracking (*i.e.*, basal plane facet formation) of recrystallized α grains. The fracture surface of internal crack initiation sites (region I) consisted of two regions, A and B (Figure 10). We surmised that a microcrack nucleated in a recrystallized α grain near its β boundary (region A) and grew transgranularly into a facet as a fatal crack (region B). The internal crack initiation sites are judged to stage I crack. Stage I is defined as short and mixed-mode crystallographic cracks, while stage II is long cracks growing *via* a plastic blunting or a ductility exhaustion mechanism. The size of internal crack initiation site increased from a few tens of microns to about 100 μm as peak cyclic stress decreased.[12] It may depend on the "ΔK_{lmax} = constant" relationship to the internal crack size, basically controlled by the transition from stage I to stage II.[5,7,11] Thus, at lower stress level, a

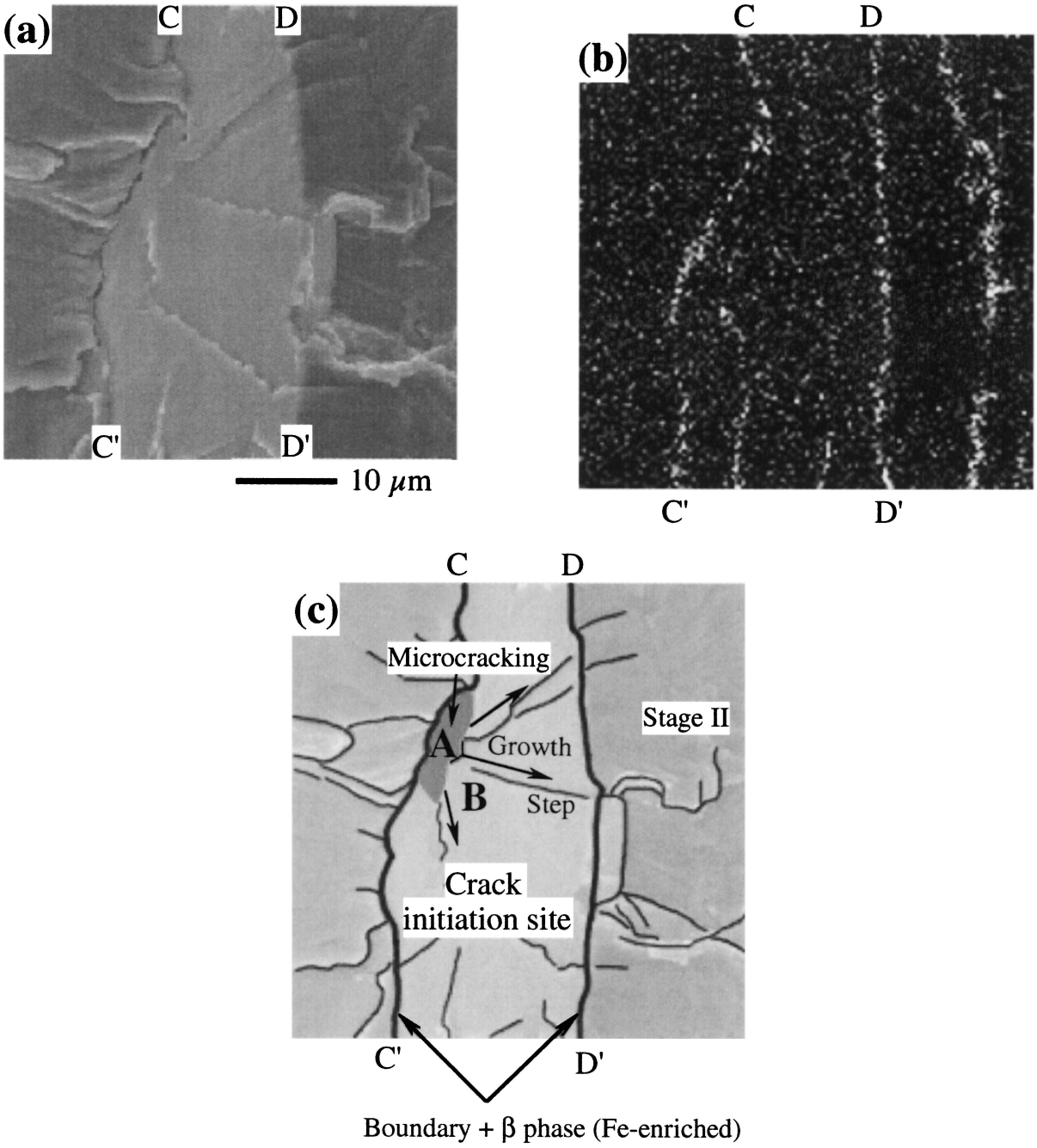

Fig. 11—Iron mapping by EDS at the internal crack initiation site in Fig. 10 (b): (*a*) secondary electron image, (*b*) iron mapping image, and (*c*) illustration.

facet grew and/or coalesced with neighboring facets into one larger site, as shown in Figure 12. The internal crack initiation sites, therefore, were produced as a mixed mode stage I crack. Evidently, internal fatigue crack generation occurs in the absence of defects such as microvoids and inclusions as well as in other titanium alloys[5,10,14,15,34,35] and austenitic steels,[7] and microcracking in an α grain and its growth agrees well with those of Ti-6Al-4V alloys in the previous study.[5]

Steele and McEvily[34] studied fatigue failure of Ti-6Al-4V alloy in the high-cycle range at stress well below the macroyield range, showing that internal stress intensification was responsible for crack initiation rather than surface roughening by slip bands and that the number of mobile dislocations increased to cause cyclic softening. Feaugas and Clavel[36] reported that cyclic softening results from a decreased back-stress component.

A simple explanation we can reach is that pre-existing dislocations in recovered α grains multiply themselves and dislocation structures are rearranged through cyclic deformation. Thus, the recovered α grain region behaves as a "softer" region than recrystallized α grains in cyclic deformation at very low stress level. Development of sub-boundaries in a recovered α grain under cyclic deformation (Figure 15) is

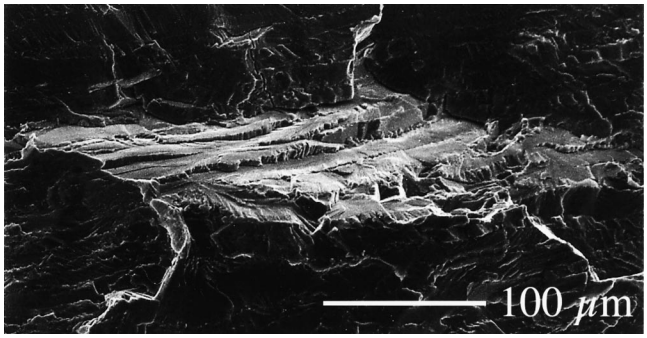

Fig. 12—SEM photograph of an internal crack initiation site (σ_{max} = 646 MPa, N_f = 5,107,910 cycles).

a Bauschinger effect, which is another evidence of softening structure. On the other hand, almost no plastic deformation of the sample was detected macroscopically. We assume that cyclic deformation did not produce a change of the shape for recovered α grains, and the arrays are *geometrically necessary (GN)* dislocations.[37] Therefore, screw dislocations on a single-slip system cause a shear strain field against neighboring grains near the boundaries. Evans and Bache[38] point out that quasi-cleavage facets are the result of stress redistribution between weak (easy slip) and strong (difficult slip) regions in the near α titanium alloy, since the applied stress is less than the macroscopic yield stress.

On the other hand, the absence of dislocation sources explains why no slip occurred in recrystallized α grains at such a low stress level. We first assume an ideal crystal for the recrystallized α grain. Resistance due to atomic force between the nearest atomic planes is a function of relative displacement, x. Hooke's law gives applied shear stress:

$$\tau_a = \mu \frac{x}{d} \qquad [3]$$

where d is distance to the nearest neighbor. The simplest function of τ_a, is

$$\tau_a = k \cdot \sin\left(\frac{2\pi x}{b}\right) \qquad (x << b) \qquad [4]$$

Then Eqs. [3] and [4] approximately give applied shear stress as

$$\tau_a = \frac{b}{d}\frac{\mu}{2\pi} \cdot \sin\left(\frac{2\pi x}{b}\right) \qquad [5]$$

In Eq. [5], maximum stress, τ_c, can be calculated as

$$\tau_c \cong \frac{\mu}{2\pi} = 6.3 \times 10^9 \ (\mathrm{N/m^2}) \left(x = \frac{b}{4},\ b \cong d\right)$$

According to a more accurate approximation by Mackenzie, $\tau_c = \mu/30$,[39] τ_c is 1.3×10^9 (N/m^2).

Second, what is the level of the critical resolved shear stress (CRSS) for α-titanium single crystal? The CRSS of the $\{01\bar{1}0\}-\langle 11\bar{2}0\rangle$ slip below 300 K increases dramatically as temperature decreases.[31,32] Furthermore, screw dislocations move more slowly than edge dislocations,[40] tending to be straight at low temperatures, which suggests that lattice friction controls flow stress at low temperatures. At low

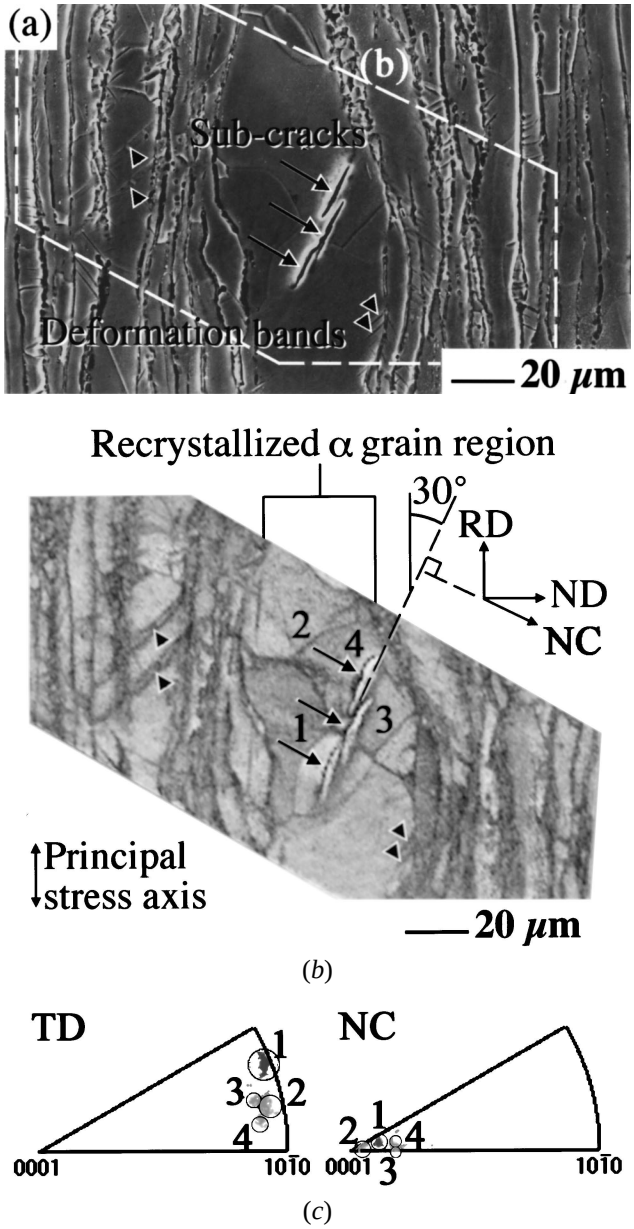

Fig. 13—Subcracks formed in a recrystallized α grain (σ_{max} = 1033 MPa, N_f = 47,130 cycles): (*a*) secondary electron image, (*b*) its EBSP image quality map, and (c) inverse pole figures for EBSP readings taken from the region of subcracks. Arrows and arrowheads indicate subcracks and deformation (slip) bands, respectively. Areas 1, 2, 3, and 4 marked in (b) denote the typical regions of EBSP readings for discrete plots in (c). The NC in (b) is normal to the inclination of subcracks and rotates by 30 deg clockwise from the ND with the TD axis.

temperature, therefore, relaxation of stress by secondary slips such as $\{0001\}-\langle 11\bar{2}0\rangle$ and $\{01\bar{1}1\}-\langle 11\bar{2}1\rangle$ in the hexagonal α phase is much more difficult than that at room temperature. Under fatigue deformation and fracture, these facts clearly produce dislocation arrays on a single-slip system and make clear the presence of weak microstructural links. The effects of temperature are common in other near α titanium alloys.[2,5,6] The CRSS of titanium containing oxygen with 2690 ppm is estimated about 1.5×10^8 (N/m^2) at 77 K.[40] Thus, the CRSS is estimated to be about $\mu/265$.

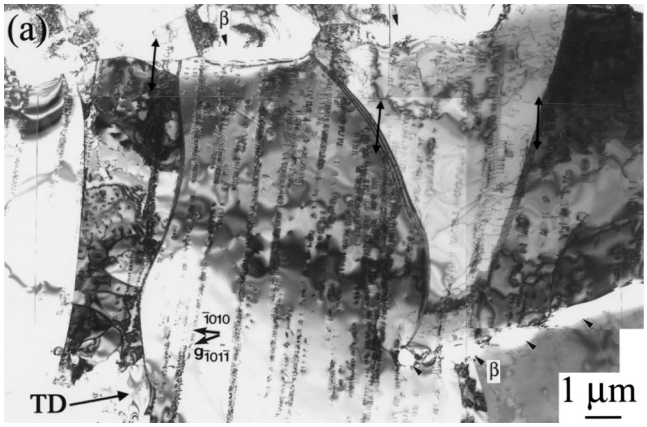

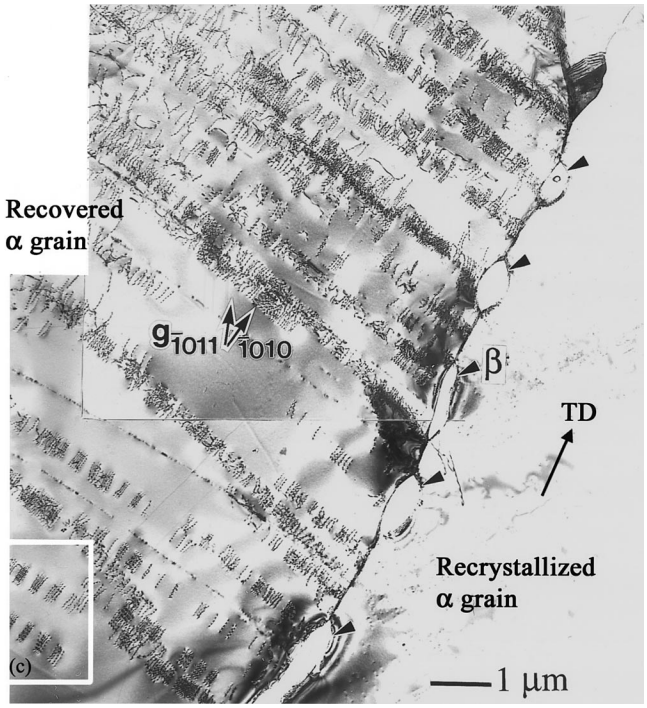

(*b*)

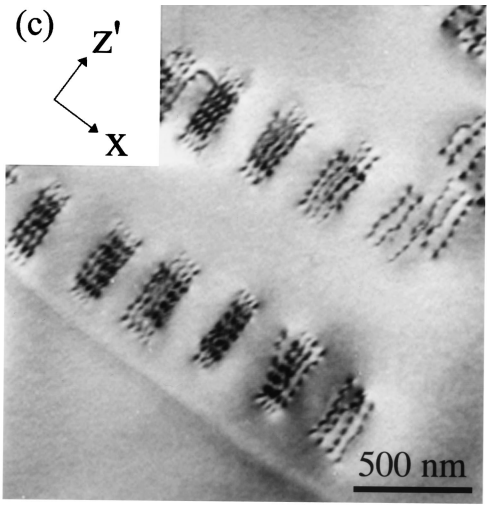

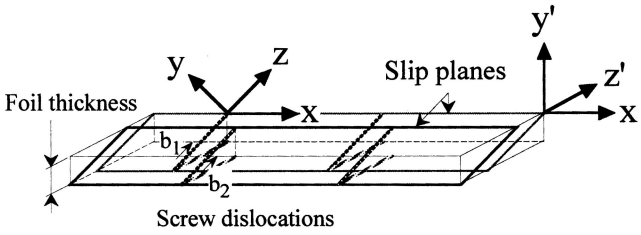

Fig. 14—Dislocation structure in the recovered α grain region after cyclic deformation (σ_{max} = 995 MPa, N_f = 75,740 cycles). Arrowheads in photographs (*a*) and (*b*) indicate β phases. Arrows in photograph (a) show slip transfer at sub-boundaries. Photograph (*c*) is a magnified image of photograph (b) and shows stacked dislocations.

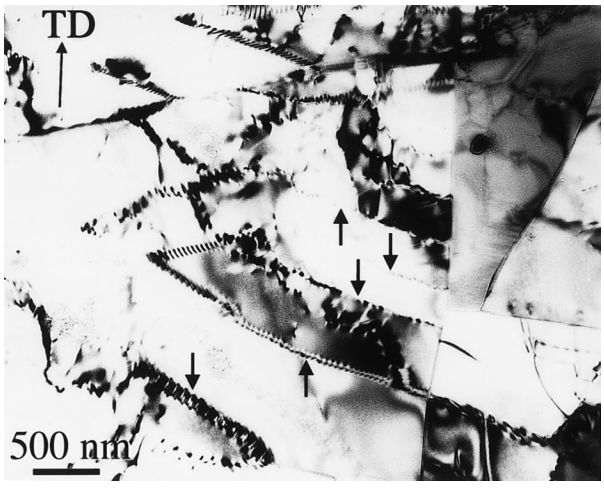

Fig. 15—Subgrain structure in the recovered α grain region after cyclic deformation (σ_{max} = 904 MPa, $N_f = 1.7 \times 10^6$ cycles). Beam direction is near $(12\bar{3}0)$.

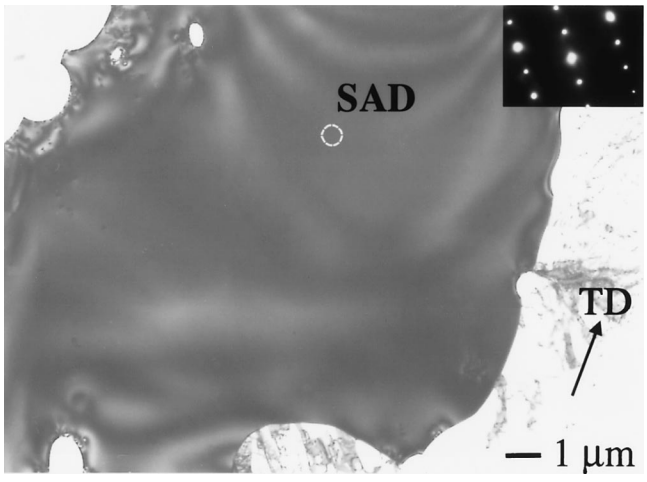

Fig. 16—TEM photograph of a recrystallized α grain after cyclic deformation (σ_{max} = 995 MPa, N_f = 75,740 cycles). Beam direction is near $(01\bar{1}0)$ normal at marked area of SAD.

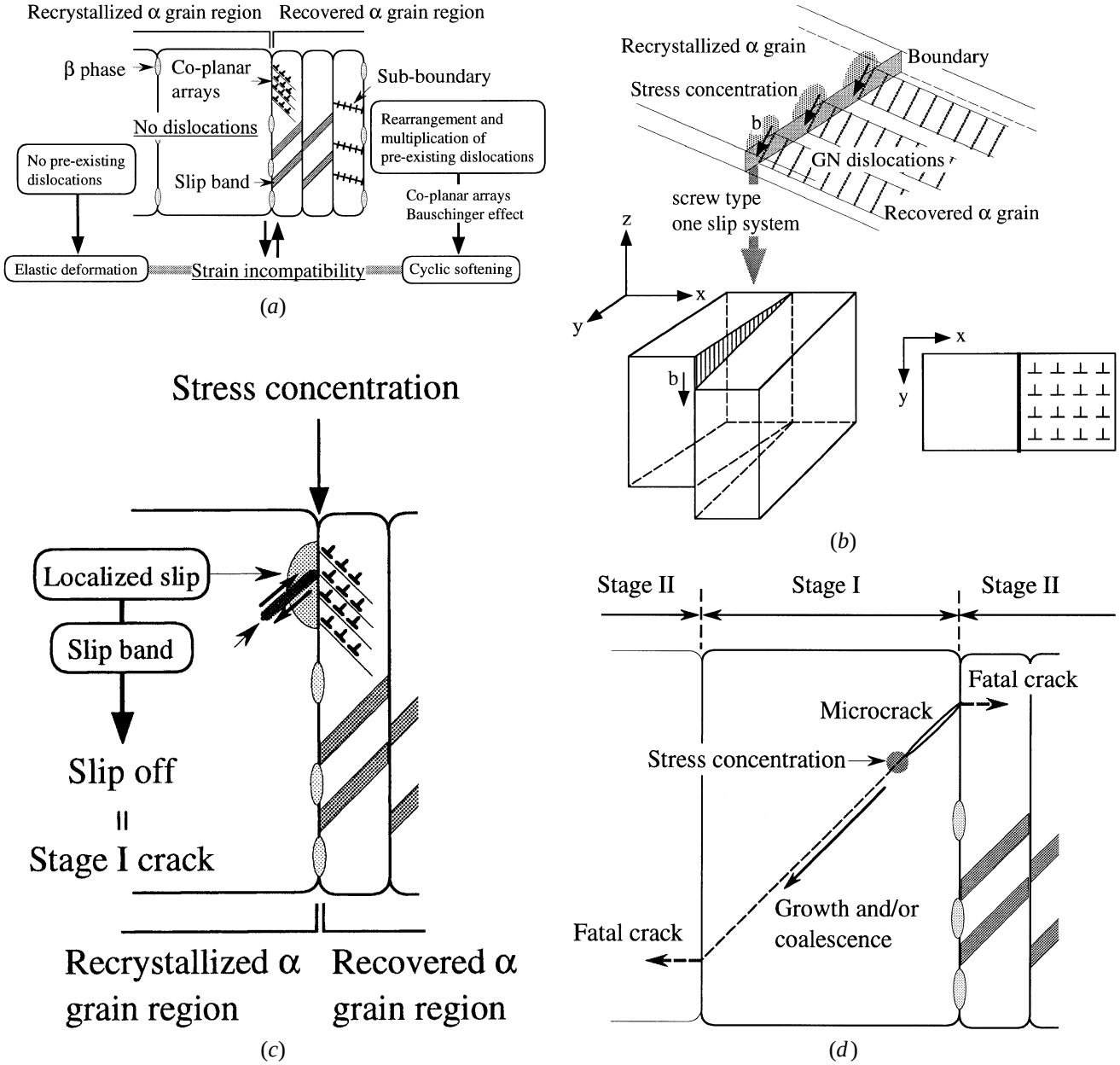

Fig. 17—Illustrations of internal fatigue crack generation in Ti-Fe-O alloy: (*a*) cyclic deformation structure, (*b*) stress concentration, (*c*) local yielding, and (*d*) growth of microcrack.

Next we estimate the stress concentration level. Assume n screw dislocations in a single-ended coplanar array spread over region $0 < x < L$ with the same sign. The shear stress, τ_a, is given as[41]

$$\tau_a = \frac{nb}{\pi L}\,\mu \qquad [6]$$

Figure 14(b) shows about 100 dislocations in a coplanar array over 10 μm including stacked dislocations. In this case, τ_a is about $\mu/1069 = 3.7 \times 10^7$ (N/m^2) and is lower than the CRSS at the edge of the recovered α grain region. However, the total shear stress should be a combination of the applied stress and the *compatibility* stresses. In addition, dislocations are only of the $\langle a \rangle$ type on prismatic planes. Thus, there are no constituents of plastic deformation along $\langle c \rangle$ axis with respect to the hexagonal crystal lattice.

To relax the strain incompatibility, a slip or microcracking must locally yield the recrystallized α grain. It has been suggested that facet formation requires a critical combination of shear stress and tensile stress on the basal slip plane.[33,38] When a slip is introduced in a recrystallized α grain, the slipped plane becomes softer than nonslipped area due to an increase in mobile dislocations. Hence, necessary slips may be localized near the first slip plane. This localized slip plane, *e.g.*, basal plane, may be the softest from the viewpoint of crystallographic orientation. Shear strain field is believed to have a characteristic orientation closely related with the applied stress axis, since the microstructures have some textures related with rolling direction. Actually, slip bands were detected in a recrystallized α grain near the boundary with the recovered α grain region in Figure 13(a). And tensile stress normal to the slip plane is active, since there

are no constituents of plastic deformation along the $\langle c \rangle$-axis. Thus, the localized slip following slip off, which was noted in the Fujita model[42] is a model to relax the strain incompatibility instead of brittle cracking[43] such as cleavage. In this model, however, a slip on the basal plane must be activated in a recrystallized α grain. Microcrack growth may also depend on the localized slip plane (slip bands), because the localized slip plane must be related with a specific crystal plane, *e.g.*, primary slip plane and/or conjugate ones. Then the model can explain why regions A and B appeared on the internal fatigue crack initiation site (Figure 10) and why their inclination with respect to the principal stress axis was almost the same. Therefore, essential features of the model are illustrated schematically in Figure 17 for the internal fatigue crack generation of Ti-Fe-O.

- Coplanar arrays in recovered α grains are GN dislocations. Thus, at the boundary between recovered α grain and recrystallized α grain, a strain incompatibility may increase due to the rearrangement of dislocation structure in recovered α grains (Figure 17(a)).
- This strain incompatibility produces local stress concentration in the recrystallized α grain (Figure 17(b)). A combination of the shear stress and tensile stress normal to the slip plane (*i.e.*, basal plane) may give a trigger of the internal fatigue crack generation.
- Slips in the recrystallized α grain are localized near the first slip plane and produce a slip band (Figure 17(c)). The slip band results in slip off (microcrack), which relaxes the stress concentration in the recrystallized α grain.
- Microcrack growth in the recrystallized α grain region also depends on the localized slip plane (Figure 17(d)). The microcrack growth and/or coalesce occur as a mixed mode crack.

V. CONCLUSIONS

We studied the microstructure and the internal fatigue crack initiation sites of Ti-Fe-O alloy, with the following results.

1. The alloy consisted of a recovered α grain region and recrystallized α grain one. Beta grains, where iron was enriched, were isolated and distributed along α grain boundaries. Dislocations were detected in recovered α grains, but not in recrystallized α grains.
2. The internal crack initiation site formed transgranularly and was related to a recrystallized α grain region, judging from its size, morphology, chemistry, and subcrack observation. Traces or steps in the initiation site showed that microcracking and its growth in recrystallized α grain region generated the site. Facets of subcracks had a near basal plane orientation with respect to the hexagonal crystal lattice.
3. Dislocation arrays or sub-boundary structures generated by cyclic deformation were seen in recovered α grains. Coplanar slip on $\{01\bar{1}0\} - \langle 11\bar{2}0 \rangle$ system occurred predominantly, and dislocation movements were restricted to slip planes. Almost no dislocations occurred in recrystallized α grains. Thus, the recovered α grain region softened.
4. A model of the internal fatigue crack generation was proposed. A strain incompatibility at grain boundaries may increase due to the rearrangement of dislocation structure. This strain incompatibility produces a local stress concentration in the neighboring recrystallized α grain. A combination of the shear stress and tensile stress normal to the slip plane (*i.e.*, basal plane) is considered a potential source of microcracking.

ACKNOWLEDGMENTS

We thank Dr. K. Tsuzaki, NRIM, and Professor T. Ohashi, Kitami Institute of Technology, for their invaluable discussion.

REFERENCES

1. M. Klesnil and P. Lukas: *Fatigue of Metallic Materials*, 2nd ed., Elsevier, Amsterdam, 1992, p. 84.
2. O. Umezawa and K. Nagai: *Iron Steel Inst. Jpn. Int.*, 1997, vol. 37, pp. 1170-79.
3. W.A. Wood: in *Fatigue in Aircraft Structures*, A.M. Freudenthal, ed., Academic Press, New York, NY, 1956, p. 1.
4. P. Neumann: *Acta Metall.*, 1969, vol. 17, pp. 1219-25.
5. O. Umezawa, K. Nagai, and K. Ishikawa: in *Fatigue' 90*, H. Kitagawa and T. Tanaka, eds., Mater. Component Eng. Pub., Birmingham, United Kingdom, 1990, vol. 1, pp. 267-72.
6. O. Umezawa, K. Nagai, and K. Ishikawa: *Mater. Sci. Eng.*, 1990, vol. A129, pp. 217-21.
7. O. Umezawa and K. Nagai: *Metall. Mater. Trans. A*, 1998, vol. 29A, pp. 809-22.
8. J.T. Fourie: *Phil. Mag.*, 1968, vol. 17, pp. 735-56.
9. I.R. Kramer, C.R. Fong, and B. Wu: *Mater. Sci. Eng.*, 1986, vol. 80, pp. 37-48.
10. S. Adachi, L. Wagner, and G. Lütjering: in *Titanium Science and Technology*, G. Lütjering, U. Zwicher, and W. Bunk, eds., Deutsche Gesellschaft für Metallkunde, Oberursel, 1985, vol. 4, pp. 2139-46.
11. O. Umezawa and K. Ishikawa: *Mater. Sci. Eng. A*, 1994, vol. A176, pp. 397-403.
12. H. Yokoyama, O. Umezawa, K. Nagai, and T. Suzuki: *Iron Steel Inst. Jpn. Int.*, 1997, vol. 37, pp. 1237-44.
13. T. Shindo, T. Watanabe, and M. Kondo: *Proc. Int. Conf. on Titanium Products and Applications*, Titanium Development Association, Boulder, CO, 1990, p. 469.
14. J. Ruppen, P. Bhowal, D. Eylon, and A.J. McEvily: *Fatigue Mechanisms*, Special Technical Publication 675, ASTM, Philadelphia, PA, 1978, pp. 47-68.
15. D.F. Neal and P.A. Blenkinsop: *Acta Metall.*, 1976, vol. 24, pp. 59-63.
16. S.I. Hong and C. Laird: *Acta Metall. Mater.*, 1990, vol. 38, pp. 1581-94.
17. V. Gerold and H.P. Karnthaler: *Acta Metall.*, 1989, vol. 37, pp. 2177-83.
18. O. Umezawa, K. Nagai, H. Yokoyama, and T. Suzuki: in *High Cycle Fatigue of Structural Materials*, W.O. Soboyejo and T.S. Srivatsan, eds., TMS, Warrendale, PA, 1997, pp. 287-98.
19. M. Peters, A. Gysler, and G. Lütjering: *Metall. Trans. A*, 1984, vol. 15A, pp. 1597-1605.
20. O. Umezawa, K. Nagai, and K. Ishikawa: *Mater. Sci. Eng. A*, 1990, vol. A129, pp. 223-7.
21. T. Ogata and K. Ishikawa: *Trans. Iron Steel Inst. Jpn.*, 1986, vol. 26, pp. 48-52.
22. T. Ogata, K. Ishikawa, K. Nagai, T. Yuri, and O. Umezawa: *Cryogenic Eng.*, 1991, vol. 26, pp. 190-96 (in Japanese).
23. T.A. Manson and B.L. Adams: *JOM*, 1994, vol. 46, pp. 43-45.
24. H. Yokoyama, O. Umezawa, K. Nagai, T. Suzuki, and K. Kokubo: *Titanium '99 Sci. Technol.*, 2000, in press.
25. A.N. Stroh: *Proc. R. Soc. London, Ser. A*, 1954, vol. 223, p. 404.
26. C. Sarrazin, R. Chiron, S. Lesterlin, and J. Petit: *Fatigue Fract. Eng. Mater. Struct.*, 1994, vol. 17, pp. 1383-9.
27. R.J. Wilson, M.R. Bache, and W.J. Evans: in *Small Fatigue Cracks, Mechanics, Mechanisms and Applications*, K.S. Ravichandran, R.O. Ritchie, and Y. Murakami eds., Elsevier Science, New York, NY, 1999, pp. 199-206.
28. M.R. Bache, W.J. Evans, and H.M. Davies. *J. Mater. Sci.*, 1997, vol. 32, pp. 3435-42.
29. D.L. Davidson and D. Eylon: *Metall. Trans. A*, 1980, vol. 11A, pp. 837-43.

30. D. Shechtman and D. Eylon: *Metall. Trans. A*, 1978, vol. 9A, pp. 1018-20.
31. E.D. Levine: *Trans. AIME*, 1966, vol. 236, pp. 1558-64.
32. M.P. Biget and G. Saada: *Phil. Mag. A*, 1989, vol. 59, pp. 747-57.
33. C.C. Wojcik, K.S. Chan, and D.A. Koss: *Acta Metall.*, 1988, vol. 36, pp. 1261-70.
34. R.K. Steele and A.J. McEvily: *Eng. Fract. Mech.*, 1976, vol. 8, pp. 31-37.
35. R. Chait and T.S. DeSisto: *Metall. Trans. A*, 1977, vol. 8A, pp. 1017-20.
36. X. Feaugas and M. Clavel: *Acta Mater.*, 1997, vol. 45, pp. 2685-2701.
37. M.F. Ashby: *Phil. Mag.*, 1970, vol. 21, pp. 399-424.
38. W.J. Evans and M.R. Bache: *Int. J. Fatigue*, 1994, vol. 16, pp. 443-52.
39. J.K. Mackenzie: Ph.D. Thesis, Bristol University, Bristol, United Kingdom, 1949.
40. S. Naka, A. Lasalmonie, P. Costa, and L.P. Kubin: *Phil. Mag. A*, 1988, vol. 57, pp. 717-40.
41. D. Hull and D.J. Bacon: *Introduction to Dislocations*, 3rd ed., Pergamon Press, Elmsford, NY, 1984, p. 208.
42. F. E. Fujita: *Acta. Metal.*, 1958, vol. 6, pp. 543-51.
43. P. Hansen: *Physical Metallurgy*, 2nd ed., Cambridge University Press, Cambridge, United Kingdom, 1986, p. 306.